Free Radical Biology and Medicine 67 (2014) 437–450

Contents lists available at ScienceDirect

Free Radical Biology and Medicine

journal homepage: www.elsevier.com/locate/freeradbiomed

Original Contribution

A mitochondria-targeted mass spectrometry probe to detect glyoxals: implications for diabetes ☆

Pamela Boon Li Pun [a], Angela Logan [a], Victor Darley-Usmar [b], Balu Chacko [b], Michelle S. Johnson [b], Guang W. Huang [b], Sebastian Rogatti [a], Tracy A. Prime [a], Carmen Methner [c], Thomas Krieg [c], Ian M. Fearnley [a], Lesley Larsen [d], David S. Larsen [d], Katja E. Menger [a], Yvonne Collins [a], Andrew M. James [a], G.D. Kishore Kumar [e], Richard C. Hartley [e], Robin A.J. Smith [d], Michael P. Murphy [a,*]

[a] MRC Mitochondrial Biology Unit, Wellcome Trust/MRC Building, Cambridge CB2 0XY, UK
[b] Department of Pathology, Centre for Free Radical Biology, University of Alabama at Birmingham, Birmingham, AL 35294, USA
[c] Department of Medicine, University of Cambridge, Addenbrooke's Hospital, Cambridge CB2 2QQ, UK
[d] Department of Chemistry, University of Otago, Dunedin, New Zealand
[e] Centre for the Chemical Research of Ageing, WestCHEM School of Chemistry, University of Glasgow, Glasgow G12 8QQ, UK

ARTICLE INFO

Article history:
Received 3 August 2013
Received in revised form
22 November 2013
Accepted 25 November 2013
Available online 4 December 2013

Keywords:
Mitochondria
Exomarker
Methylglyoxal
Glyoxal
Hyperglycemia
MitoG
Free radicals

ABSTRACT

The glycation of protein and nucleic acids that occurs as a consequence of hyperglycemia disrupts cell function and contributes to many pathologies, including those associated with diabetes and aging. Intracellular glycation occurs after the generation of the reactive 1,2-dicarbonyls methylglyoxal and glyoxal, and disruption of mitochondrial function is associated with hyperglycemia. However, the contribution of these reactive dicarbonyls to mitochondrial damage in pathology is unclear owing to uncertainties about their levels within mitochondria in cells and in vivo. To address this we have developed a mitochondria-targeted reagent (MitoG) designed to assess the levels of mitochondrial dicarbonyls within cells. MitoG comprises a lipophilic triphenylphosphonium cationic function, which directs the molecules to mitochondria within cells, and an *o*-phenylenediamine moiety that reacts with dicarbonyls to give distinctive and stable products. The extent of accumulation of these diagnostic heterocyclic products can be readily and sensitively quantified by liquid chromatography–tandem mass spectrometry, enabling changes to be determined. Using the MitoG-based analysis we assessed the formation of methylglyoxal and glyoxal in response to hyperglycemia in cells in culture and in the Akita mouse model of diabetes in vivo. These findings indicated that the levels of methylglyoxal and glyoxal within mitochondria increase during hyperglycemia both in cells and in vivo, suggesting that they can contribute to the pathological mitochondrial dysfunction that occurs in diabetes and aging.

Glycation, the nonenzymatic formation of sugar–protein and sugar–nucleotide adducts, plays a major role in disrupting cell function and causing tissue damage in a range of pathologies such as diabetes, aging, and neurodegeneration [1–3]. Glycation increases in response to the elevation in glucose that occurs in unregulated diabetes and is a major cause of diabetic complications [4,5]. Within the cell excessive glucose can lead to molecular damage through the formation of 1,2-dicarbonyl compounds such as methylglyoxal from the triose phosphate intermediates of glycolysis [1,6] or from the metabolism of acetone generated during ketosis [7]. These reactive 1,2-dicarbonyls often exist in modified chemical forms in situ including reversible hemiacetals, hemithioacetals, and hemiaminals with small biomolecules and with reactive moieties on proteins and nucleic acids [8,9]. In addition they can react directly with free amine functions on proteins and nucleic acids, thereby generating substantial permanent modifications such as arginine-derived hydroimidazolones and lysine cross-links on proteins [10] and guanine-derived imidazopurinones on DNA [11]. Such modifications are thought to result in biochemical dysfunction by altering protein structure and activity and by inducing genomic mutations [2]. These markers of glycation damage are elevated in many clinical samples from diabetic patients and also in animal models of diabetes and aging [2,4,9,12,13], consistent with a contribution from these reactions to cell damage and pathology.

* Corresponding author.
E-mail address: mpm@mrc-mbu.cam.ac.uk (M.P. Murphy).

0891-5849/$ - see front matter © 2013 The Authors. Published by Elsevier Inc. All rights reserved.
http://dx.doi.org/10.1016/j.freeradbiomed.2013.11.025

An important role for methylglyoxal and glyoxal in pathology is further supported by the existence of the glyoxalase enzyme system, which specifically degrades these two dicarbonyls [14]. Loss of the glyoxalase degradation pathway renders organisms more susceptible to glycation and subsequent damage, whereas its overexpression increases life span in *Caenorhabditis elegans* [15]. Thus dicarbonyl-associated glycation of proteins and nucleic acids is a significant contributing factor in a range of pathologies, particularly those associated with diabetes or aging.

In hyperglycemia, there is considerable evidence for mitochondrial damage and elevated oxidative stress that contribute to pathology, and this has been in part ascribed to mitochondrial glycation due to methylglyoxal and glyoxal [16–21]. Furthermore these reactive dicarbonyls disrupt mitochondrial function in vitro [22–24]. Therefore, understanding the contribution from glycation damage by reactive dicarbonyls to mitochondrial dysfunction is important for analyzing and understanding the pathology associated with hyperglycemia. However, the mechanistic details are uncertain, and it has proven difficult to specifically evaluate the importance of these processes. This is in part due to the uncertainties related to the distribution of methylglyoxal and glyoxal between the cytosol and the mitochondria. To assess the importance of mitochondrial damage caused by methylglyoxal and glyoxal we have developed a mitochondria-selective molecule, MitoG, to assess relative changes in the levels of these damaging species within mitochondria in cells and in vivo.

To target mitochondria we used the lipophilic triphenylphosphonium (TPP) cation functionality, which has been shown to direct a wide variety of antioxidants, probes, and bioactive molecules to mitochondria in cells, animal models, and patients after intravenous, oral, or intraperitoneal administration [25–27]. Uptake occurs directly through the phospholipid bilayer and does not require a protein carrier. The extent of accumulation in mitochondria is determined by the membrane potential and can be adequately described by the Nernst equation, which indicates an ~10-fold increase in accumulation per 60 mV membrane potential under

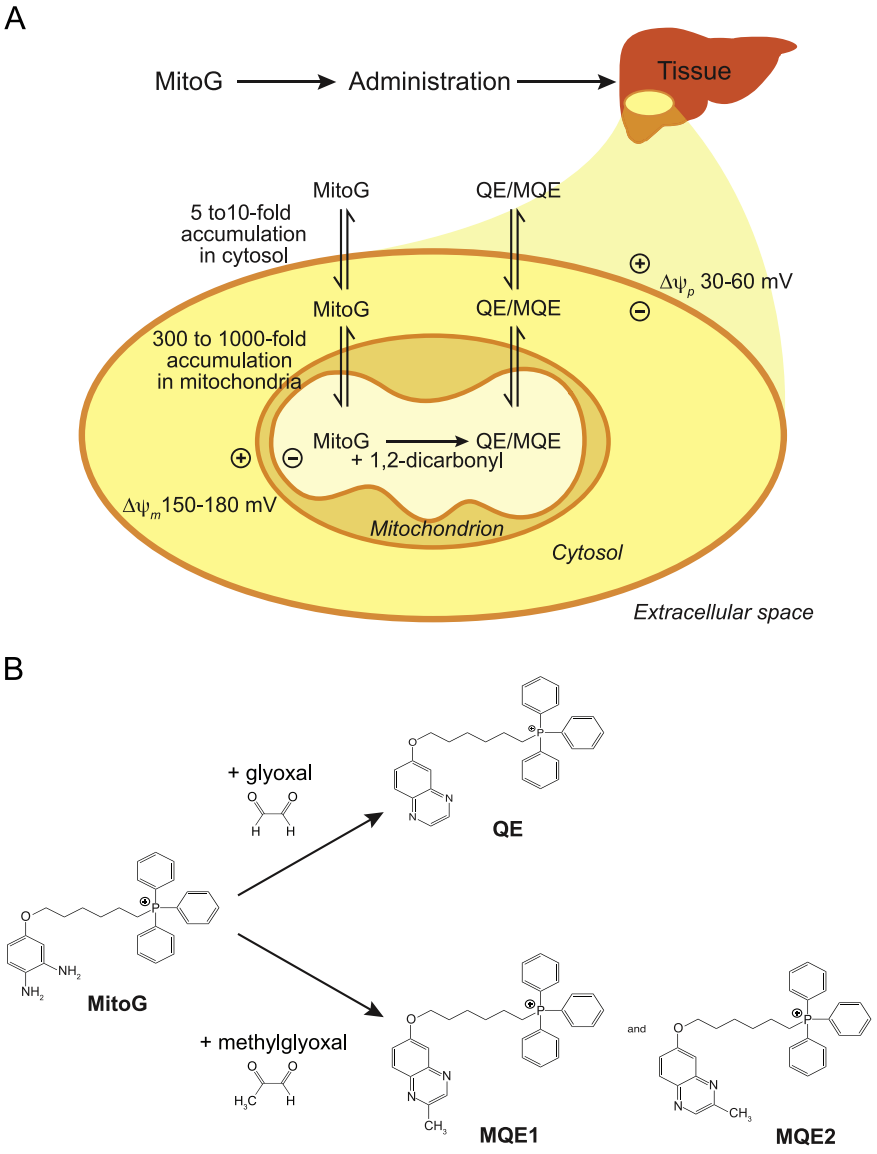

Fig. 1. Rationale and mechanism for the detection of intramitochondrial dicarbonyls. (A) MitoG, a mitochondria-targeted glyoxal and methylglyoxal trap, consists of a mitochondria-targeting TPP moiety and a phenylenediamine group that reacts with 1,2-dicarbonyls. The TPP moiety of MitoG leads to its uptake into tissues where it accumulates within mitochondria, driven by both the plasma and the mitochondrial membrane potentials. (B) Within mitochondria MitoG can then react with glyoxal or methylglyoxal to form the quinoxaline products, QE and MQE (present as two isomers, MQE1 and MQE2). These products can then be quantified by LC–MS/MS relative to deuterated internal standards to provide a measure of the amount of free glyoxal and methylglyoxal present within mitochondria in cells and in vivo.

typical biological conditions [25–27]. Consequently, TPP compounds accumulate ~1000-fold within mitochondria in vivo assuming plasma and mitochondrial membrane potentials of 30 and 160 mV, respectively [25–27] (Fig. 1A).

Alkoxy-substituted phenylenediamines have been used for detecting 1,2-dicarbonyls because of the enhanced reactivity due to the electron-donating alkoxy substituent [28,29]. These are commonly used derivatizing agents for the detection of dicarbonyls, reacting to form stable quinoxaline products [12,13,28]. Therefore, to make a mitochondria-targeted molecule that reacts selectively with methylglyoxal and glyoxal, we conjugated the TPP moiety through an oxygen atom to an *o*-phenylenediamine moiety. The mode of action of this molecule, called MitoG, is shown in Fig. 1B. The ability to quantify the accumulation of the quinoxaline products from the in situ reaction of MitoG with methylglyoxal and glyoxal provides an opportunity to assess changes in the levels of these compounds in mitochondria in cells and in vivo. This can be done by an extension of an approach we recently developed to assess levels of mitochondrial hydrogen peroxide in vivo by the use of a mitochondria-targeted peroxide reactive compound, MitoB [30,31]. In this methodology, a diagnostic exomarker product, MitoP, was formed from MitoB, and its levels were determined ex vivo by liquid chromatography–tandem mass spectrometry (LC–MS/MS) of tissue homogenates relative to deuterated internal standards [30,31]. The sensitivity of such an approach is greatly enhanced by the inherent positive charge of the TPP moiety that decreases the threshold for detection by MS, enabling the analysis of fmol compound/g wet wt tissue [30,31]. Thus relative changes in methylglyoxal and glyoxal levels within mitochondria can be assessed based upon the extent of accumulation of the MitoG–dicarbonyl quinoxaline reaction products (Fig. 1B). Here we describe the development of MitoG, a mitochondria-targeted probe for methylglyoxal and glyoxal. We show that it can be used for the evaluation of 1,2-dicarbonyl production within mitochondria in cells and in vivo. These findings are consistent with mitochondrial glycation contributing to the underlying pathology of hyperglycemia in diabetes and related disorders.

Materials and methods

Chemical syntheses

A schematic of the syntheses of MitoG, quinoxaline ether (QE), and the methylquinoxaline ethers 1 and 2 (MQE1/MQE2) is shown in Fig. 2. In summary, 6-(4-aminophenoxy)hexanol (**1**) was synthesized using the reported method [32]. Nitration of **1** was achieved as described [33] and involved conversion of **1** to the acetamide followed by nitration with concentrated nitric acid to give **2.** Deprotection then gave the nitroaniline **3** in 48% overall yield from **1.** The basic *o*-phenylenediamine skeleton was obtained by catalytic hydrogenation of the nitroaniline **3** over palladium on carbon. The air- and light-sensitive diamine **4** was immediately protected with *tert*-butyloxycarbonyl (Boc) groups by treatment with di-*tert*-butyldicarbonate in tetrahydrofuran [34]. The primary alcohol in **5** was mesylated to give **6** and then converted to the phosphonium functional group by reaction with triphenylphosphine and sodium iodide in acetonitrile. The product **7** was obtained by precipitation from ether and column chromatography to give a white solid in 80% yield. To obtain a robust analytical

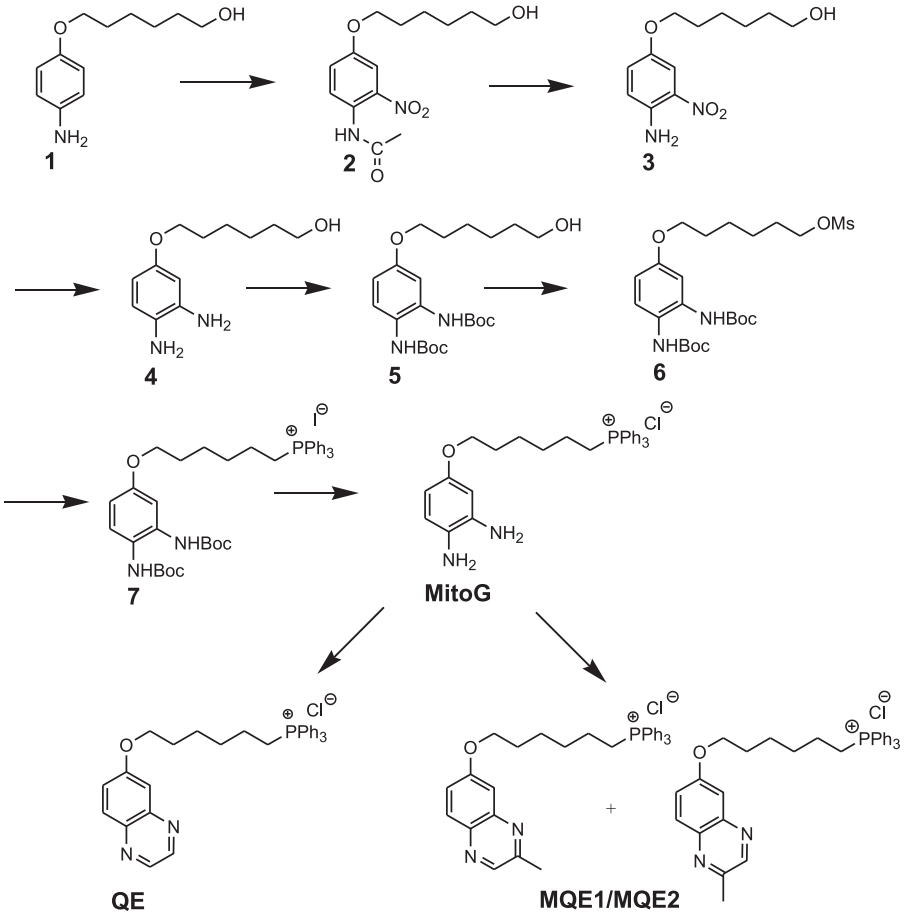

Fig. 2. Syntheses of MitoG, MQE, and QE. A detailed description of the synthetic procedures and product characterization and yields for all the reactions is given in the supplementary materials.

sample, anion exchange to the tetraphenylborate was carried out by treatment of **7** with sodium tetraphenylborate in dichloromethane. Deprotection of the amino groups to give MitoG was accomplished by treatment of **7** in 1,4-dioxane with 9.8 M hydrochloric acid. MitoG was then reacted with either glyoxal to give the quinoxaline QE or with methyl glyoxal to give the two methylquinoxaline products, MQE1 and MQE2, which were formed in a ratio of 10:1 (by ^{1}H NMR), although they gave a single HPLC peak. Data are quoted for the major isomer. Further details of the syntheses, including the associated synthesis of 4-hexyloxyphenylene-1,2-diamine (HP), are given in the supplementary material.

The glyoxalase I inhibitor, bromobenzyl glutathione cyclopentyl diester, was synthesized by alkylation of glutathione [35], followed by standard Boc protection, coupling with cyclopentanol using 2-(1*H*-benzotriazole-1-yl)-1,1,3,3-tetramethyluronium tetrafluoroborate [36], trifluoroacetic acid (TFA) removal of the Boc group, and treatment with sodium bicarbonate to give the free base. Other reagents were obtained from Sigma–Aldrich, unless otherwise stated. ^{1}H, ^{13}C, and ^{31}P spectra were acquired on Varian INOVA-400 or Varian INOVA-500 spectrometers. Chemical shifts are reported downfield from TMS, relative to the solvent residual signal. For the chemical synthesis components of this work, high-resolution mass spectra were recorded on a Bruker microTOF electrospray mass spectrometer and HPLC analysis was carried out on an Agilent HP1100: column Phenomenex Prodigy 250 × 3 mm, gradient elution 10% acetonitrile/water (0.1% TFA) to 100% acetonitrile over 12.5 min at 0.5 ml min^{-1} with detection at 210 and 254 nm.

Assessment of compound properties

TPP-conjugated compounds were made up as 10 mM stock solutions in dimethyl sulfoxide (DMSO), flushed with argon, and stored as aliquots at −20 °C. UV/visible spectra and kinetic analyses were done using a Shimadzu UV-2501PC spectrophotometer in a 1-ml cuvette containing KCl buffer (120 mM KCl, 10 mM Hepes, and 1 mM EGTA, pH 7.2 (KOH)). The molar extinction coefficients were calculated from the absorbance at maximal absorption (λ_{max}) for the compounds for solutions of known concentration. Reaction rates between MitoG and 1,2-dicarbonyls were determined from the initial linear slope over the first 30 s at the λ_{max} for the formation of the relevant quinoxaline. Fluorescence spectra were obtained in 2.5 ml KCl buffer using a Shimadzu RF-301PC fluorimeter with slit widths of 3 nm. Kinetic assays used excitation and emission wavelengths of 344 and 433 nm, respectively; emission spectra used an excitation wavelength of 344 nm and excitation spectra used an emission wavelength of 433 nm.

RP-HPLC was performed using a Gilson 321 pump with a C18 column (Jupiter 300 Å, Phenomenex) with a Widepore C18 guard column (Phenomenex). Samples (1 ml) were injected through a 0.22-μm polyvinylidene difluoride (PVDF) filter (Millex, Millipore). HPLC buffer A (0.1% TFA in water) and HPLC buffer B (90% acetonitrile and 0.1% TFA) were used and a gradient was run at 1 ml/min at room temperature as follows: 0–2 min, 5% B; 2–17 min, 5–100% B; 17–19 min, 100% B; 19–22 min, 100–5% B. Peaks were detected by absorbance at 220 nm (UV/Vis 151; Gilson) and by fluorescence (excitation and emission wavelengths of 344 and 433 nm; RF-10AXL; Shimadzu). Partition coefficients between phosphate-buffered saline (PBS) and octan-1-ol were determined as previously described [37].

Mitochondrial preparation and incubations

Rat liver mitochondria (RLM) were prepared at 4 °C in STE buffer (250 mM sucrose, 5 mM Tris, and 1 mM EGTA, pH 7.4 (HCl)) by homogenization and differential centrifugation. Protein concentration was determined using the biuret assay relative to bovine serum albumin and was typically 40–60 mg/ml. A Clark-type oxygen electrode (Rank Brothers, Bottisham, Cambridge, UK) connected to a Powerlab 2/20 data acquisition system (ADInstruments, Bella Vista, NSW, Australia) was used to measure respiration rates and was calibrated with air-saturated water (210 nmol O_2/ml at 37 °C). RLM (2 mg protein/ml) were suspended in 120 mM KCl, 10 mM Hepes, 1 mM EGTA, 1 mM $MgCl_2$, and 5 mM KH_2PO_4, pH 7.2 (KOH) in a thermostated 1-ml electrode chamber with stirring. MitoG was then added and after 5 min glutamate and malate (5 mM each) were added, followed 3 min later by 400 μM ADP. Oxygen consumption rates were determined from the slopes using Chart version 5.5.6. for Mac (ADInstruments). An electrode selective for the TPP moiety of MitoG was constructed and used as previously described [38].

Cell culture

All cells were incubated at 37 °C in a humidified atmosphere of 95% air and 5% CO_2 and culture media used were supplemented with 10% (v/v) fetal calf serum (FCS), 100 U/ml penicillin, and 100 μg/ml streptomycin. C2C12 cells (mouse myoblast cell line; European Collection of Animal Cell Cultures) were cultured in low-glucose (1000 mg/L D-glucose) Dulbecco's modified Eagle's medium (DMEM; Invitrogen). Cells were maintained at subconfluency (< 80%) to prevent differentiation. BAECs (bovine aortic endothelial cells; Cell Applications, San Diego, CA, USA) were maintained in α-minimum essential medium (Invitrogen) containing 5 mM D-glucose. All culture flasks and assay plates used for experiments were precoated with fibronectin (25 μg/ml; Sigma) in Hanks' balanced salt solution (Cell Applications) at 1–4 μg fibronectin/cm^2. After 1 h at room temperature excess coating solution was removed, and flasks and plates were then seeded with cells for experiments. BAECs were used for experiments at passages 4–6.

To assess cell viability, C2C12 cells or BAECs were seeded at a density of 10,000 or 40,000 cells/well, respectively, in 96-well plates. After an overnight incubation, the medium was replaced with fresh medium containing test compounds and incubated for 24 h. To determine cell survival, cells were washed twice with medium, then fresh medium (100 μl per well) was added and mixed with 20 μl 3-(4,5-dimethylthiazol-2-yl)-5-(3-carboxymethoxyphenyl)-2-(4-sulfophenyl)-2*H*-tetrazolium (MTS)/phenazine methosulfate (Promega, Madison, WI, USA). After 2 h absorbance was read at 490 nm in a plate reader (SpectraMax Plus 384; Molecular Devices). All treatments were conducted in triplicate wells.

The Seahorse XF24 extracellular flux analyzer was used to assess cellular oxygen consumption rate (OCR) [39–41]. Cells (40,000 BAECs/well) were cultured and subjected to experimental treatment in Seahorse XF24 V7 assay plates that were coated with fibronectin as described above. OCR was determined as follows: cells were washed twice in assay medium (4.15 g/L DMEM base, 1.85 g/L NaCl, 1 × Glutamax (Invitrogen), 1 mM sodium pyruvate, 5 mM D-glucose, 15 mg/L phenol red, 20 mM Hepes, and 0.4% (v/v) FCS, pH 7.4) and incubated in 630 μl of assay medium for 1 h at 37 °C in air. After 20 min equilibration, basal OCR was determined, and after 3 h incubation with MitoG, OCR was determined after sequential injections of oligomycin (1 μg/ml), carbonylcyanide *p*-trifluoromethoxyphenylhydrazone (FCCP; 2 μM), and rotenone/antimycin A (4 μg/ml and 5 μM, respectively). OCRs were normalized to cell number as measured using the sulforhodamine B (SRB) assay as follows: cells were fixed (200 μl of 5% trichloroacetic acid at 4 °C for 1 h), washed with water (3 ×), stained for 20 min with 50 μl of 0.4% (w/v) SRB in 1% (v/v) acetic acid, and washed (3 × 1% acetic acid) and the incorporated SRB dye was solubilized in 100 μl of 10 mM Tris base for 5 min. Then 50 μl of each sample was transferred in duplicate to a 96-well plate and mixed with 50 μl of

10 mM unbuffered Tris base and absorbance was read at 565 nm in a plate reader (SpectraMax Plus 384; Molecular Devices). A standard curve was constructed by seeding a known number of cells in quadruplicate wells and fixing and staining them in parallel with sample wells. To calculate the proportion of oxygen consumption attributable to proton leak and reserve capacity, OCRs after injection of oligomycin, FCCP, and rotenone/antimycin A were expressed as a percentage of the total basal OCR [40,42].

To assess total methylglyoxal formation in cells by RP-HPLC, the cell layers were washed in PBS (1 ml), scraped into 1.5 ml PBS, and pelleted by centrifugation (16,000*g* for 2 min). The cell pellet was resuspended in 500 μl KCl buffer, 500 μl 0.1% formic acid was added, the protein was pelleted by centrifugation as above, and the supernatant was collected. Methylglyoxal was then derivatized to 2-methylquinoxaline by addition of 100 μM *o*-phenylenediamine followed by incubation at 37 °C for 4 h. Samples were dried under vacuum and assessed for 2-methylquinoxaline as previously described [28]. Briefly, dried samples were resuspended in 1 ml HPLC buffer (68% (v/v) 10 mM KH_2PO_4, pH 2.5, and 32% acetonitrile), filtered (0.22-μm PVDF; Millex; Millipore), and separated by isocratic RP-HPLC in the HPLC buffer above at a flow rate of 2 ml/min at room temperature using a Gilson 321 pump with a C18 column (Jupiter 300 Å; Phenomenex) and a Widepore C18 guard column (Phenomenex). Peaks were detected fluorimetrically (excitation and emission wavelengths of 352 and 385 nm, respectively; RF-10AXL; Shimadzu).

For LC–MS/MS analysis of MitoG reaction products cells were incubated in T25 flasks (Nunc) with 2 μM MitoG at 37 °C. Cell monolayers were washed (1 ml PBS), scraped into 1.5 ml PBS, and pelleted by centrifugation (16,000*g* for 2 min). The pellet was resuspended in 250 μl 100% acetonitrile/0.1% spiked with deuterated internal standards (ISs; 100 pmol each d_{15}-MQE and d_{15}-QE), vortexed, and centrifuged (2 × 16,000*g* for 15 min). Samples were dried under vacuum (Savant SpeedVac), resuspended in 100 μl 20% acetonitrile/0.1% formic acid, vortexed, centrifuged (16,000*g* for 10 min), transferred to silanized autosampler vials (Chromacol 1.5HRRV(S)), flushed and sealed under argon, and then stored at −80 °C until LC–MS/MS analysis.

Where specified, cells were subjected to acute glycemia treatment and were incubated in low-glucose (5 mM D-glucose), high-glucose (30 mM D-glucose), or osmotic control medium (5 mM D-glucose + 25 mM L-glucose) for 4 h.

Mouse experiments

The Akita mouse model of type I diabetes ($Ins2^{+/-Akita J}$) [43–45] was assessed at the University of Alabama. All procedures were performed in accordance with *Guide for the Care and Use of Laboratory Animals* and were approved by the Institutional Animal Care and Use Committee at the University of Alabama at Birmingham. Male $Ins2^{+/-Akita J}$ and wild-type (C57BL/6) mice (4–8 weeks of age) from The Jackson Laboratory (Bar Harbor, ME, USA) were maintained on laboratory chow and water ad libitum until 14 weeks of age, when they were used for experiments. For this MitoG (100 nmol in 100 μl saline) was administered by tail vein injection. After 4–6 h the mice were killed and urine samples taken and snap-frozen for subsequent analysis of MQE/QE content. Blood glucose levels were measured using an Accu-Chek Advantage blood glucose meter (Roche Diagnostics). Urine creatinine levels were determined at the Core Biochemical Assay Laboratory (Addenbrooke's Hospital, Cambridge, UK). To extract MQE and QE, 20 μl urine was mixed with 500 μl 60% acetonitrile/0.1% formic acid and incubated on ice for 30 min. The extracts were then spiked with deuterated ISs (100 pmol each d_{15}-MQE and d_{15}-QE), vortexed for 30 s, incubated on ice for 30 min with vortexing every 10 min, and then centrifuged (16,000*g* for 10 min). The supernatants were collected, filtered (0.22-μm PVDF; Millex; Millipore), and dried under vacuum (Savant SpeedVac). The dried samples were resuspended in 150 μl 20% acetonitrile/0.1% formic acid by vortexing for 5 min, followed by centrifugation at 16,000*g* for 10 min. Samples were then transferred to silanized autosampler vials (Chromacol 1.5HRRV(S)), flushed and sealed under argon, and stored at −80 °C until LC–MS/MS analysis.

LC–MS/MS analysis

The MS fragmentation patterns of TPP compounds were determined by direct infusion of compounds (1 μM in 20% acetonitrile (v/v)) at 2 μl/min into a triple-quadrupole mass spectrometer (Waters Quattro Ultima). Electrospray ionization in positive ion mode was used with the following settings: source spray voltage, 3 kV; cone voltage, 100 V; ion source temperature, 80 °C; collision energy, 50 V. Nitrogen and argon were used as the curtain and collision gas, respectively.

LC–MS/MS analyses were carried out using a triple-quadrupole mass spectrometer (Waters Xevo TQ-S) with an I-class Aquity LC system (Waters) attached. Samples were kept at 4 °C before injection by the autosampler of 10 μl into a 15-μl flow-through needle and RP-HPLC at 30 °C using a Luna 5 μ Phenyl-Hexyl column (1 × 50 mm, 5 μm; Phenomenex) with a Phenyl-Hexyl guard column (2 × 4 mm; Phenomenex). Buffers used were MS buffer A (0.1% (v/v) formic acid in water) and MS buffer B (95% acetonitrile/0.1% formic acid (both v/v)). A gradient was run at 50 μl/min as follows: 0–2 min, 5% B; 2–3 min, 5–25% B; 3–5 min, 25–75% B; 5–7 min, 75–100% B; 7–10 min, 100% B; 10–12 min, 100–5% B; 12–20 min, 5% B. Eluant was diverted to waste from the mass spectrometer at 0–5 and 16–20 min acquisition time using an in-line divert valve. For MS analysis, electrospray ionization in positive ion mode was used: source spray voltage, 2.5 kV; cone voltage, 25 V; ion source temperature, 100 °C; collision energy, 38 V. Nitrogen and argon were used as the curtain and the collision gas, respectively. Multiple reaction monitoring in positive ion mode was used for compound detection. Transitions used for quantification were as follows: MQE, 506 > 262; d_{15}-MQE, 521 > 277; QE, 2 > 262; and d_{15}-QE, 507 > 277. For each experiment standard curves were prepared using known amounts of MQE and QE, which were spiked with IS and extracted in parallel with the samples. Standards and samples were quantified using MassLynx 4.1 software to determine the peak area for MQE, QE, and ISs, and the standard curves were used to determine the amounts of MQE and QE present in samples.

Statistics

Data analysis was performed with the R software environment for statistical computing and graphics (R Foundation for Statistical Computing, Wien, Austria). All data were analyzed using *t* tests or one-way analysis of variance followed by post hoc Dunnett's test as appropriate and represented as the mean ± standard error of mean. *P* values equal to or less than 0.05 were taken to be statistically significant.

Results and discussion

Synthesis and characterization of MitoG and its reaction products

The syntheses of MitoG, its predicted quinoxaline products upon reaction with methylglyoxal and glyoxal, and their deuterated versions are summarized in Fig. 2. The UV/Vis absorption spectra of MitoG and its component TPP and phenylenediamine moieties are shown in Fig. 3A. As expected, the spectrum of MitoG was a summation of those of the phenylenediamine HP and a simple alkyl-TPP salt. As *o*-phenylenediamine undergoes oxidative

degradation [2], and because there was a literature precedent for the additional reactivity of alkoxy-substituted phenylenediamines, we assessed the stability of MitoG by RP-HPLC and found that stock solutions were stable under storage at −20 °C. To assess its stability under biologically relevant conditions, we measured the decomposition of dilute solutions of MitoG at 37 °C and observed

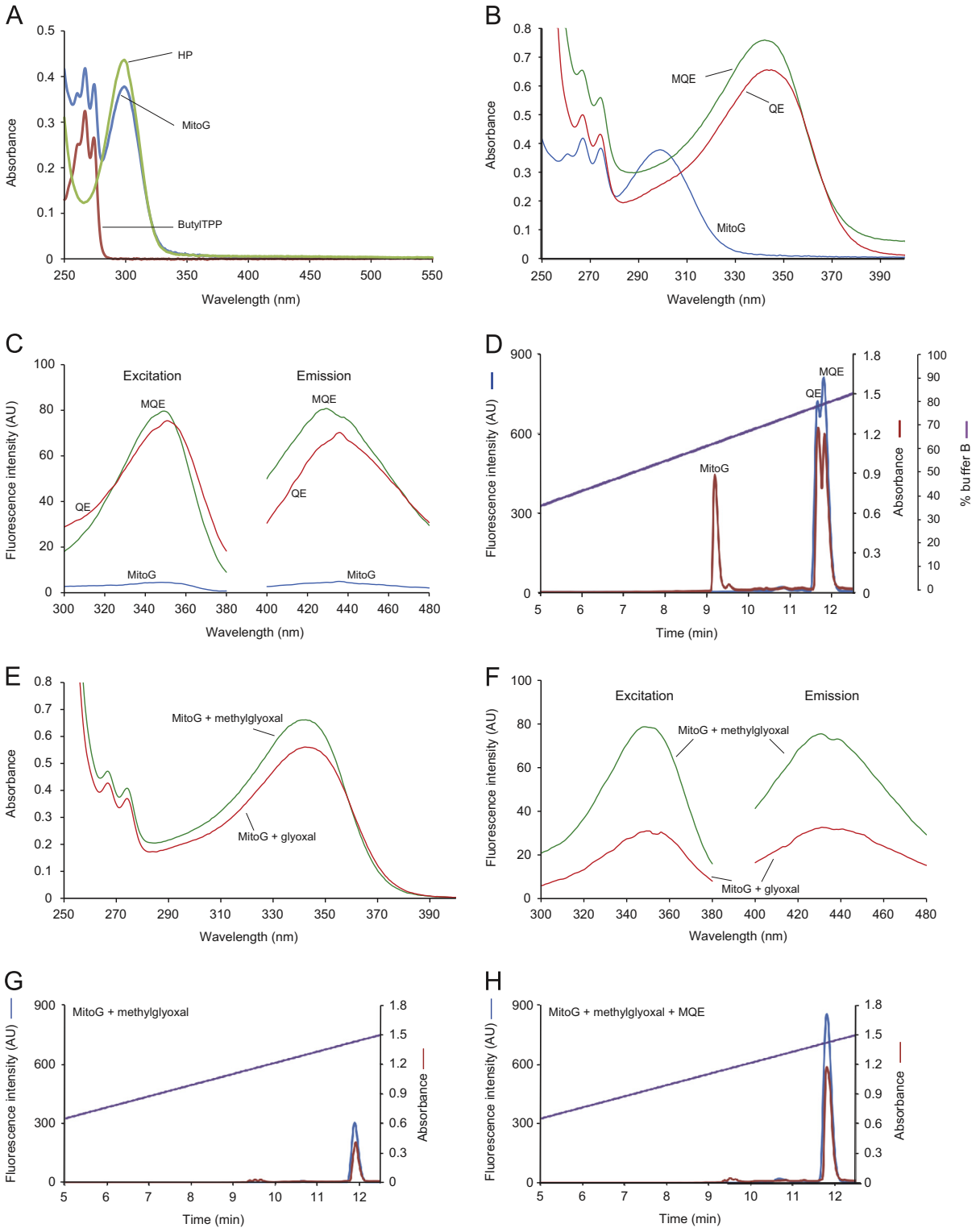

Fig. 3. In vitro characterization of MitoG, MQE, and QE. (A) UV/Vis scanning spectra of 100 μM MitoG show the characteristics of its component TPP and HP moieties. (B) UV/Vis scanning spectra of 100 μM MitoG, MQE, and QE. (C) Fluorescence excitation spectra (emission 433 nm) and emission spectra (excitation 344 nm) of 10 μM MitoG, MQE, and QE. MitoG was not fluorescent. MQE and QE had peak excitation and emission wavelengths of 344 and 433 nm, respectively. (D) RP-HPLC profile of 10 nmol each of MitoG, MQE, and QE. Absorbance (red) at 220 nm, fluorescence (blue) was observed at excitation and emission wavelengths of 344 and 433 nm, respectively. (E) UV/Vis scanning spectra of 100 μM MitoG and 1 mM methylglyoxal or glyoxal in KCl buffer after incubation at 37 °C for 2 h. (F) Fluorescence excitation and emission spectra of 10 μM MitoG and 20 μM methylglyoxal, or of 20 μM MitoG and 40 μM glyoxal, in KCl buffer after incubation at 37 °C for 2 h. (G) MitoG (5 mM) and 10 mM methylglyoxal were incubated in 10 μl KCl buffer at 37 °C for 2 h, then 1 μl of the mixture was assessed by RP-HPLC. (H) The identity of the product peak was confirmed by spiking the reaction mixture with 10 nmol of MQE standard. Experiments with glyoxal gave similar results (data not shown).(For interpretation of the references to color in this figure legend, the reader is referred to the web version of this article).

minimal loss by 4 h with significant loss by 24 h; therefore MitoG is sufficiently stable for biological experiments lasting up to ~4 h.

The expected products of the reaction of MitoG with methylglyoxal (MQE) and glyoxal (QE) were synthesized and have UV/Vis absorption spectra distinct from that of MitoG (Fig. 3B). Both QE and MQE were fluorescent, whereas MitoG was not (Fig. 3C). The three compounds were resolved by RP-HPLC (Fig. 3D) although the MQE regioisomers (MQE1, MQE2; Fig. 1B) were not distinguished. Both MQE and QE were stable after 1 week at 37 °C as assessed by RP-HPLC (data not shown). The properties of MitoG, MQE, and QE are summarized in Table 1. We conclude that MitoG is sufficiently stable for biological experiments involving trapping of glyoxal and methylglyoxal within mitochondria in cells and in vivo, and the reaction products MQE and QE were both robustly stable for chemical isolation and subsequent LC–MS/MS analyses.

Reactivity of MitoG with glyoxal and methylglyoxal

MitoG reacted with methylglyoxal and glyoxal to form products with absorption, fluorescence, and RP-HPLC properties (Figs. 3E–H) identical to those of independently synthesized and characterized MQE or QE (Figs. 3B–D). Incubation of MitoG with the biologically important and reactive aldehydes 4-hydroxynonenal and acrolein followed by RP-HPLC analysis indicated that although MitoG did react, a number of products were formed, some of which were unstable (data not shown). Thus the reaction of MitoG with these aldehydes is not diagnostically useful, in contrast to that with 1,2-dicarbonyls, which generates stable, dominant products.

Progress of the reaction between MitoG and methylglyoxal could be observed by UV/Vis spectrophotometry, but that of MitoG with glyoxal was too slow (Fig. 4A). However, both reactions could be assessed using a more sensitive fluorimetric method (Fig. 4B). The greater reactivity of methylglyoxal over glyoxal with *o*-phenylenediamines is consistent with the enhanced toxicity of methylglyoxal [46–48]. Aqueous glyoxal exists predominantly as the dihydrate, which is an unreactive tetraol, whereas methylglyoxal is predominantly the monohydrate with only the aldehyde converted into a 1,1-diol. This accounts for the greater reactivity of methylglyoxal, which requires only a single dehydration to generate the highly reactive dicarbonyl [8]. The rate constants for the MitoG–methylglyoxal and the MitoG–glyoxal reactions were 19 ± 1 and $0.6 \pm 0.3\ M^{-1}\ s^{-1}$ (means ± SE, $n=3$) at 37 °C, respectively, compared with the reported value of $1.7 \pm 0.3\ M^{-1}\ s^{-1}$ for the reaction of methylglyoxal with *o*-phenylenediamine at 25 °C [49]. A competitive rate experiment for methylglyoxal between MitoG and *o*-phenylenediamine, monitored by ^{1}H NMR (0.12 mM, DMSO, 25 °C), showed that MitoG was ~1.8 times more reactive than *o*-phenylenediamine, whereas a similar competition for glyoxal between 4-methoxyphenylene-1,2-diamine and *o*-phenylenediamine showed that the 4-methoxy substitution enhanced reactivity ~3.8-fold. Together these data confirm that MitoG reacts with 1,2-dicarbonyls to form stable diagnostic products and that the electron-donating ether linkage in MitoG enhances the reactivity compared to unsubstituted *o*-phenylenediamine.

Table 1
M extinction coefficients and partition coefficients of MitoG, MQE, and QE.

Compound	Molar extinction coefficient at wavelength λ ($M^{-1}\ cm^{-1}$)				Partition coefficient
	λ 267 nm	λ 274 nm	λ 299 nm	λ 345 nm	
MitoG	4069 ± 206	3721 ± 193	3679 ± 188		2.4 ± 0.1
MQE	6463 ± 139	5509 ± 127		7466 ± 158	12.3 ± 0.5
QE	5275 ± 293	4557 ± 245		6901 ± 375	13.6 ± 0.9

Data are means ± SE of three determinations.

Accumulation of MitoG within energized mitochondria

To be a mitochondria-selective probe for 1,2-dicarbonyls in cells and in vivo, the TPP moiety of MitoG should promote its uptake within mitochondria. We measured the uptake of MitoG by isolated mitochondria using an electrode selective for the TPP moiety of MitoG (Fig. 5). After addition of MitoG to calibrate the electrode response, subsequent addition of mitochondria led to a small decrease in MitoG concentration due to the expected adsorption of MitoG to unenergized mitochondria [38]. Addition of the respiratory substrate succinate generated a membrane potential and led to the substantial uptake of MitoG as shown by a decrease in the external concentration. Dissipation of the membrane potential with the uncoupler FCCP led to the release of MitoG from the mitochondria. The membrane potential-dependent uptake of MitoG into mitochondria was ~2 nmol/mg protein, which, assuming a mitochondrial matrix volume of 0.5 µl/mg protein [31], gives a concentration of MitoG within mitochondria of ~4 mM, whereas the external MitoG concentration was ~2 µM. This ~2000-fold accumulation of MitoG indicates that MitoG, like other TPP-conjugated compounds, is

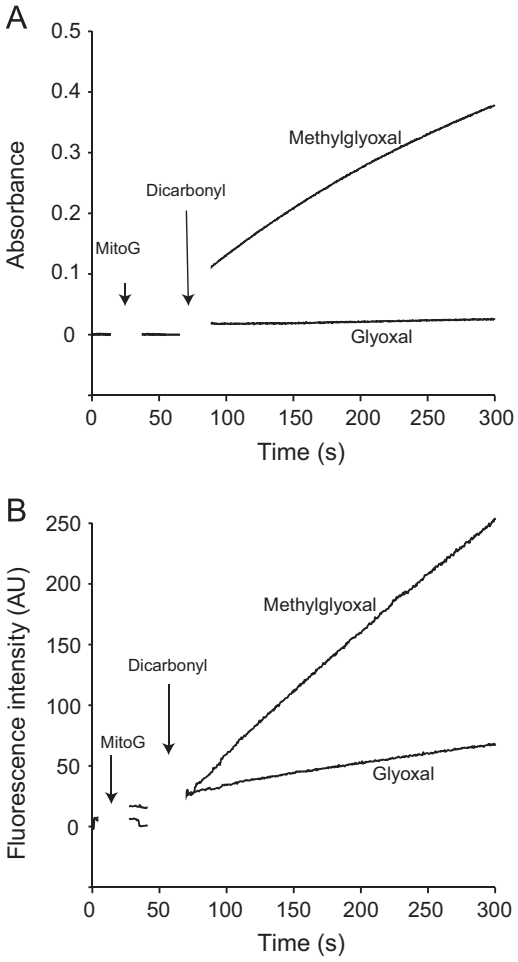

Fig. 4. In vitro reaction of MitoG with methylglyoxal and glyoxal. (A) The reactions between MitoG (100 µM) and 1,2-dicarbonyls (25 µM) at 37 °C were followed from the formation of the quinoxaline products at 345 nm. (B) Fluorimetric detection of the reaction between MitoG and methylglyoxal (40 µM each), and between MitoG and glyoxal (200 µM each), was done by monitoring the quinoxaline products at excitation and emission wavelengths of 344 and 433 nm, respectively. The changes in fluorescence caused by MQE and QE formation were quantified from calibration curves constructed by plotting fluorescence (excitation and emission wavelengths of 344 and 433 nm, respectively) against known amounts of either quinoxaline and were linear up to at least 20 µM.

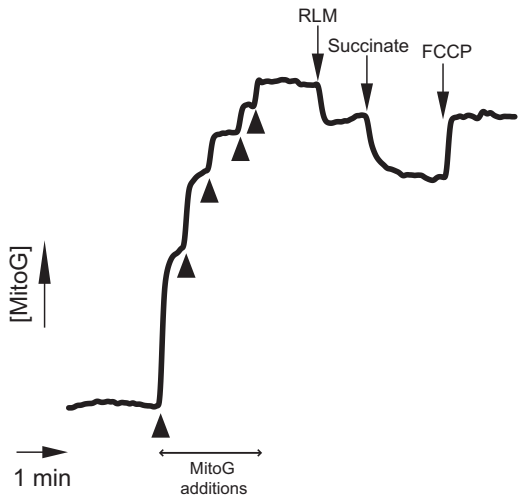

Fig. 5. Uptake of MitoG by isolated mitochondria. A TPP-selective electrode was placed in a stirred chamber at 37 °C containing 1 ml KCl buffer supplemented with 4 μg/ml rotenone. After calibration with five additions of 1 μM MitoG (arrowheads), RLM (1 mg protein/ml) were added, followed by 10 mM succinate and 500 nM FCCP where indicated. This trace is representative of three independent experiments.

selectively accumulated by mitochondria in a membrane potential-dependent manner.

For MitoG to be useful, it should not disrupt mitochondrial function or cause cell toxicity at the concentrations used. To test this we incubated MitoG with isolated mitochondria and assessed its effect on respiration under different conditions. At 5 μM MitoG there was a slight increase in proton leak as indicated by an increase in coupled respiration (Fig. 6A). This is expected as high levels of TPP cations within biological membranes eventually cause increased proton leak. In contrast, the oxidative phosphorylation complexes themselves were insensitive to MitoG up to 5 μM as there was no effect on phosphorylating respiration (Fig. 6B). MitoG only decreased the viability of C2C12 cells and BAECs at concentrations above 10 and 50 μM, respectively (Figs. 6C and D). To assess the effect of MitoG on mitochondrial function within cells, we measured the OCR using a Seahorse XF24 flux analyzer (Figs. 6E–H). Concentrations of MitoG above 10 μM slightly decreased the OCR owing to ATP synthesis, and lower concentrations in the range 2–5 μM showed a trend toward an increased OCR due to proton leak and a decreased respiratory reserve capacity. Therefore, we routinely used a MitoG concentration of 2 μM for most cell experiments.

Quantification of reaction of MitoG with 1,2-dicarbonyls by LC–MS/MS

To use MitoG to probe the local concentration of methylglyoxal and glyoxal, it was necessary to measure the amounts of the reaction products (MQE, QE) by LC–MS/MS relative to deuterated internal standards [31]. The fragmentations of MQE and QE and their deuterated versions during tandem MS were determined (Fig. 7) and were as expected for TPP compounds [31]. This fragmentation pattern —to the triphenylphosphorus cation (Fig. 8A)—was used to establish an LC–MS/MS assay for the products of the reaction of MitoG with 1,2-dicarbonyls, and typical standard curves are shown in Fig. 8B. We conclude that MitoG reaction products can be very sensitively detected, facilitating the use of MitoG to assess mitochondrial methylglyoxal and glyoxal in cells and in vivo.

MitoG as probe for mitochondrial methylglyoxal and glyoxal in cells

For MitoG to be an effective probe it should react with methylglyoxal and glyoxal within a biological system to give the diagnostic products, MQE and QE, which can then be extracted and analyzed by LC–MS/MS. To assess whether this was possible in cells, BAECs were preincubated with MitoG for 1 h, then methylglyoxal or glyoxal was added, and after a further 3 h the cell layers were extracted and analyzed by LC–MS/MS to assess the amounts of MQE (Fig. 9A) and QE (Fig. 9B). The levels of both MitoG-derived products, MQE and QE, initially increased with the concentration of exogenous 1,2-dicarbonyls added before showing saturation at supraphysiological 1,2-dicarbonyl concentrations, at which MitoG became limiting (Figs. 9A and B). Treatment with the 1,2-dicarbonyl scavenger aminoguanidine (AG), or decreasing MitoG mitochondrial uptake using the uncoupler FCCP, reduced the amounts of MQE and QE detected (Figs. 9A and B). As some MitoG is present in the culture medium, there will also be a contribution from MQE/QE formation in the supernatant that is subsequently accumulated by the cells. These findings are consistent with reaction of MitoG with methylglyoxal and glyoxal within cells to form MQE/QE and this reaction being decreased by AG or by lowering the extent of MitoG uptake into mitochondria within cells by dissipating the membrane potential. We conclude that MitoG reacts with methylglyoxal or glyoxal in a biological context to form MQE and QE and that these products can be extracted from cells and quantified by LC–MS/MS.

We next utilized MitoG to determine relative mitochondrial levels of methylglyoxal and glyoxal under hyperglycemia, a condition to which damaging glycation by 1,2 dicarbonyls is thought to contribute. First we confirmed that hyperglycemia did increase the production of cellular methylglyoxal in our system. To do this we incubated BAECs under conditions of high (30 mM) and low (5 mM) glucose for 4 h and then measured the formation of methylglyoxal by derivatization with *o*-phenylenediamine to generate 2-methylquinoxaline, which was assessed by RP-HPLC. This analysis showed that hyperglycemia in BAECs did indeed increase the formation of methylglyoxal ~2-fold compared to controls (data not shown, $n=3$). To see whether MitoG could be used to assess a change in mitochondrial methylglyoxal/glyoxal under hyperglycemic conditions we next compared the formation of MQE and QE in cells after incubation with low (5 mM) or high (25 mM) glucose for 4 h (Figs. 9C and D). There is a gradual increase in the amount of MQE detected over time and this increases substantially on going from low to high glucose, consistent with the increase in methylglyoxal within mitochondria under conditions of hyperglycemia. This formation of MQE/QE was blocked by the uncoupler FCCP (Figs. 9C and D) and the formation of MQE was also decreased by the methylglyoxal trap AG (Fig. 9E). The increase in MQE upon hyperglycemia did not occur when the high concentration of D-glucose was replaced with 25 mM nonphysiological L-glucose (along with 5 mM D-glucose to maintain cell viability). This suggests that the increase in MQE caused by a high concentration of D-glucose requires metabolism of the glucose to generate methylglyoxal and is not due to nonspecific effects of a high carbohydrate concentration in the culture medium (Fig. 9E). The reaction between MitoG and methylglyoxal/glyoxal may also occur outside mitochondria, with the subsequent uptake of MQE/QE within mitochondria. However, as the reaction between MitoG and the dicarbonyls is second order, the rate of MQE/QE formation within mitochondria is expected to be ~500- to 1000-fold greater than in other compartments, even if the methylglyoxal and glyoxal concentrations were the same. Therefore these data are consistent with the formation of MQE/QE occurring primarily within the mitochondria.

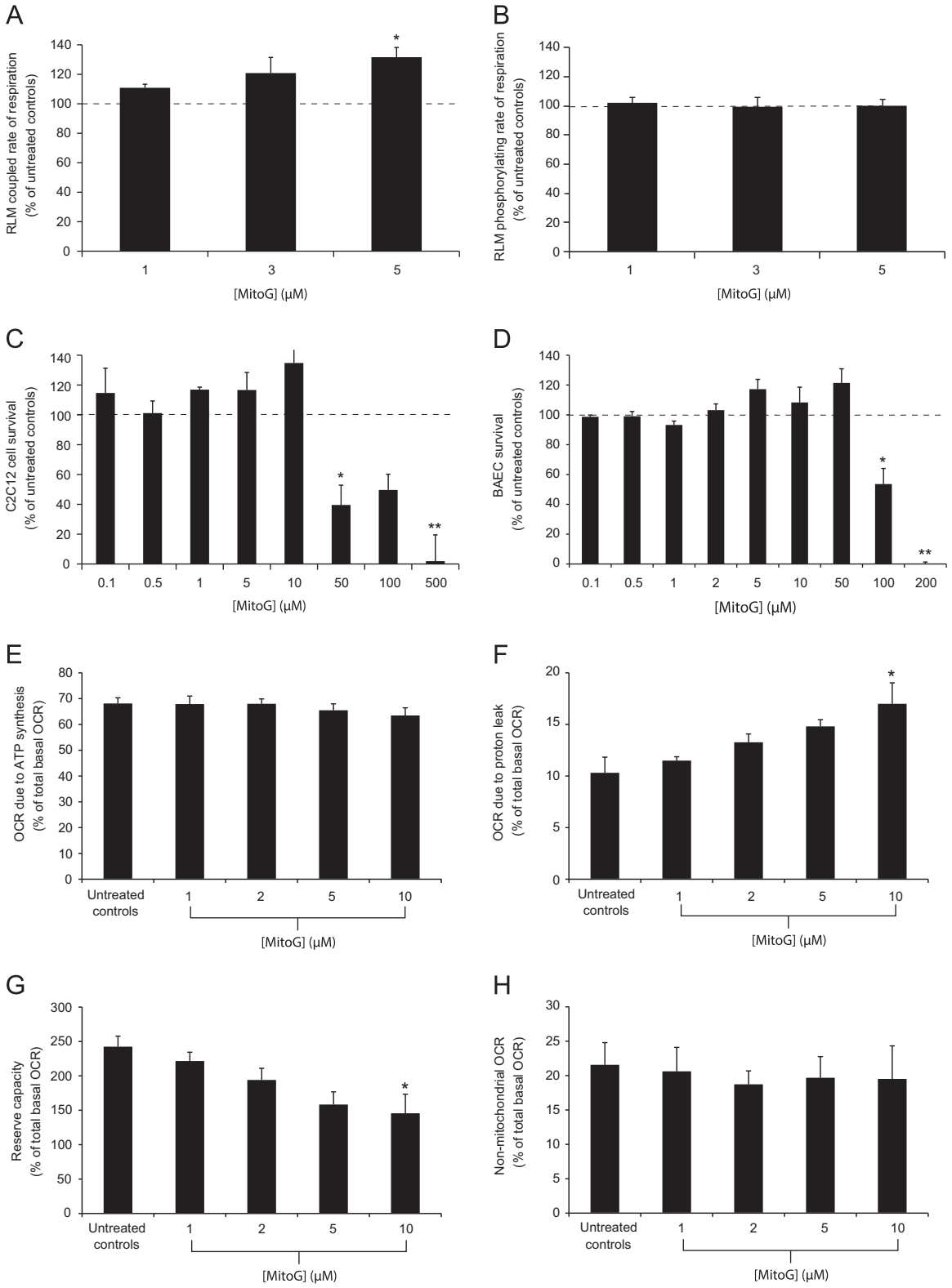

Fig. 6. Effects of MitoG on mitochondrial and cell function. (A, B) RLM respiring on glutamate/malate at 37 °C were incubated with various concentrations of MitoG for 7 min in an oxygen electrode (A) to measure coupled respiration before ADP was added (B) to measure phosphorylating respiration. Data are the percentage of the respiration rates of untreated controls (dashed lines). (C, D) (C) C2C12 cells or (D) BAECs were incubated with MitoG for 24 h and cell survival was then determined using the MTS assay. Data are expressed as a percentage of the untreated controls (dashed line). (E–H) BAECs were incubated with MitoG for 2 h at 37 °C and the cellular oxygen consumption rate (OCR) after the sequential additions of oligomycin, FCCP, and antimycin A/rotenone was then measured using a Seahorse XF24 analyzer. (E) OCR due to ATP synthesis, (F) OCR due to proton leak, (G) reserve capacity, and (H) nonmitochondrial oxygen consumption. Results are means ± SE of three independent experiments. *$P < 0.05$ or **$P < 0.01$ relative to untreated controls.

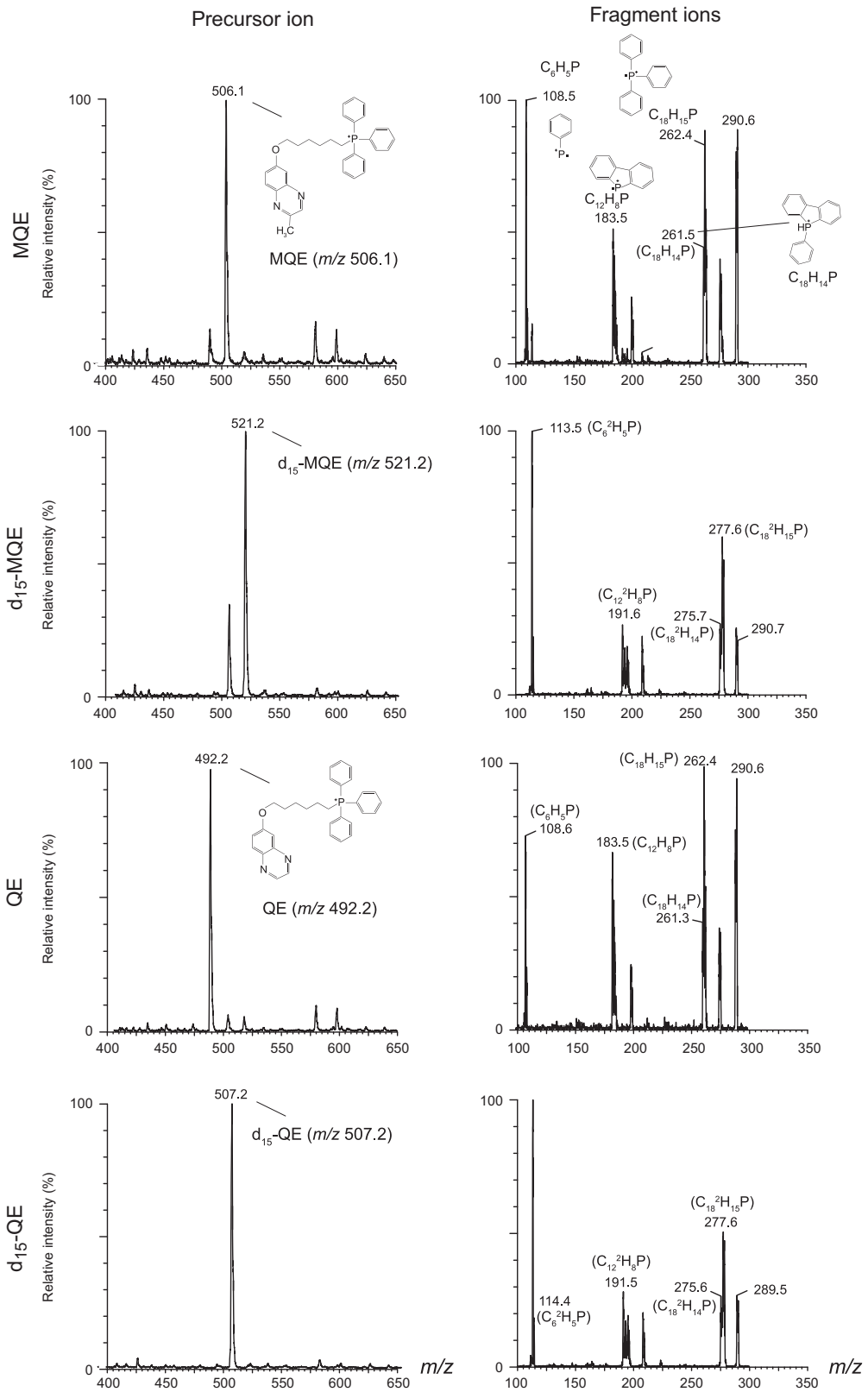

Fig. 7. Fragmentation of MQE and QE by tandem mass spectrometry. Compounds (1 μM in 20% acetonitrile) were infused, at 2 μl/min, into a triple-quadrupole mass spectrometer. The indicated parent ions of MQE and QE and their corresponding d_{15} variants were fragmented to generate the indicated daughter ions.

When BAECs were incubated under conditions of high glucose in the presence of the glyoxalase I inhibitor bromobenzyl glutathione cyclopentyl diester [35], to suppress degradation of glyoxal and methyl glyoxal, the amount of MQE and QE increased (Fig. 9F). Together these data indicate that MitoG is an effective probe for assessing changes in mitochondrial 1,2-dicarbonyl production within cells. Furthermore, these findings suggest that the mitochondrial methylglyoxal concentration increases approximately threefold under hyperglycemia. Therefore mitochondrial glycation by elevated reactive dicarbonyls is a strong candidate to contribute to the

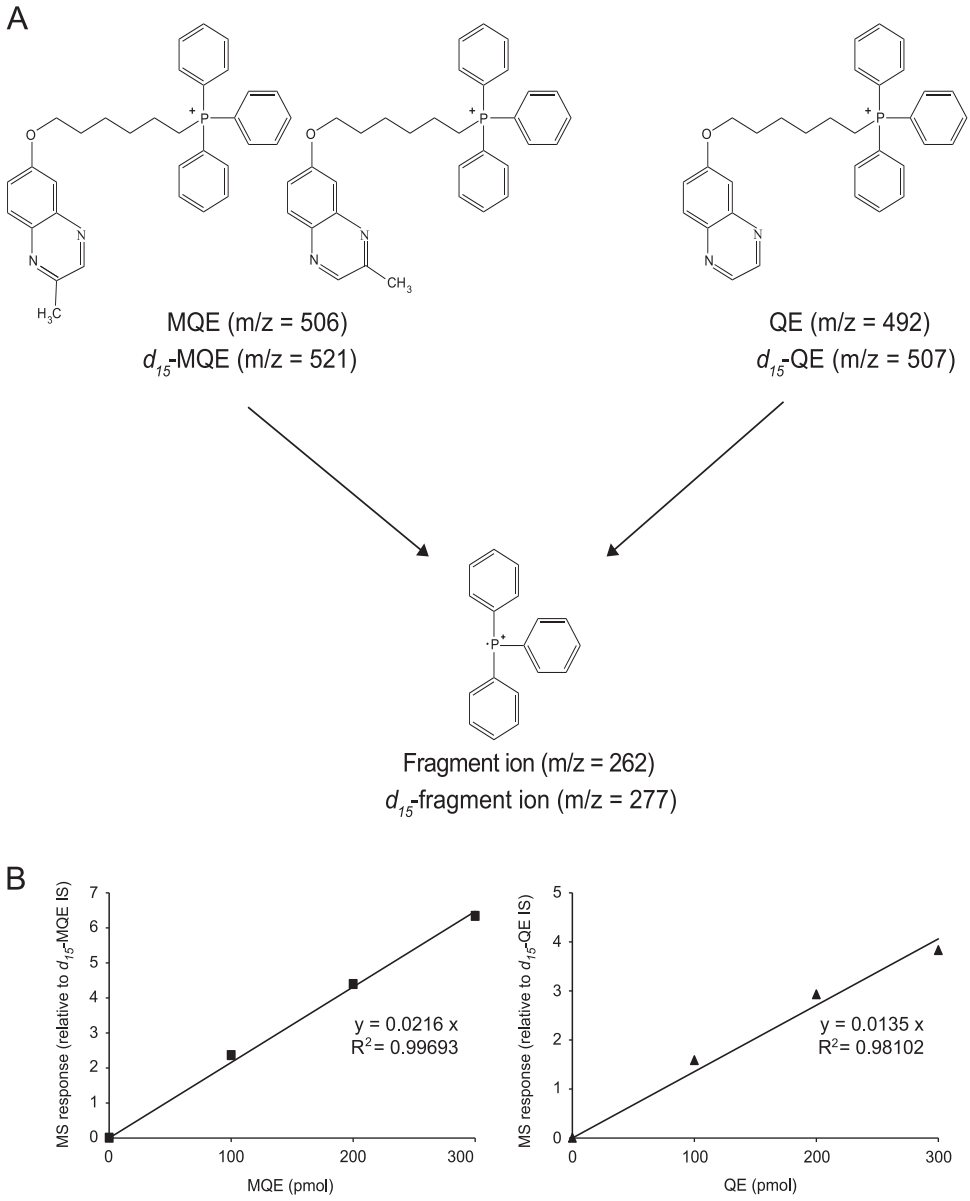

Fig. 8. LC–MS/MS analysis of MQE and QE. (A) QE and both isoforms of MQE have parent ions with distinctive *m/z* ratios that fragment to form characteristic daughter ions. (B) Standard curves based on the analyses of MQE and QE by LC–MS/MS analysis relative to the corresponding deuterated ISs.

disruption of mitochondrial function that occurs during pathological hyperglycemia.

MitoG as a probe for mitochondrial levels of methylglyoxal and glyoxal in vivo

Previously we have shown that the mitochondria-targeted hydrogen peroxide mass spectrometry probe MitoB can be used to assess the production of hydrogen peroxide within mitochondria in living fruit flies [30,31] and mice [50]. In this, MitoB is acting as a probe to generate the *exomarker* MitoP [51], which is an exogenous probe compound that when administered to an experimental animal is converted to a diagnostic marker that can be assessed ex vivo and used to infer the production of reactive species within the living organism [51]. Therefore we next set out to see if MitoG could also be used to generate the exomarkers MQE and QE to assess the formation of methylglyoxal/glyoxal within mitochondria in vivo. The TPP component of MitoG facilitates this goal, as it is known that after intravenous injection TPP compounds rapidly distribute from the blood to mitochondria within tissues and are then slowly excreted over several hours into the urine and bile [27,52,53]. Therefore it may be possible to administer MitoG to mice and then analyze urine to see if there is elevated production of the MQE/QE products under certain conditions, indicating an elevation in reactive dicarbonyls within mitochondria in vivo.

To do this we used the Akita mouse model ($Ins2^{+/-Akita}$) in which a mutation in proinsulin leads to chronic hyperglycemia and consequent pathological complications similar to those found in type I diabetes [43–45]. To assess whether there were changes in mitochondrial methylglyoxal/glyoxal in the Akita mice compared to wild type, we administered MitoG (100 nmol) as a tail vein injection and after 4–6 h urine samples were taken and the MQE and QE contents measured relative to creatinine. These data are shown as a function of blood glucose levels for individual mice (Figs. 10A and B). As expected, blood glucose was far higher in the

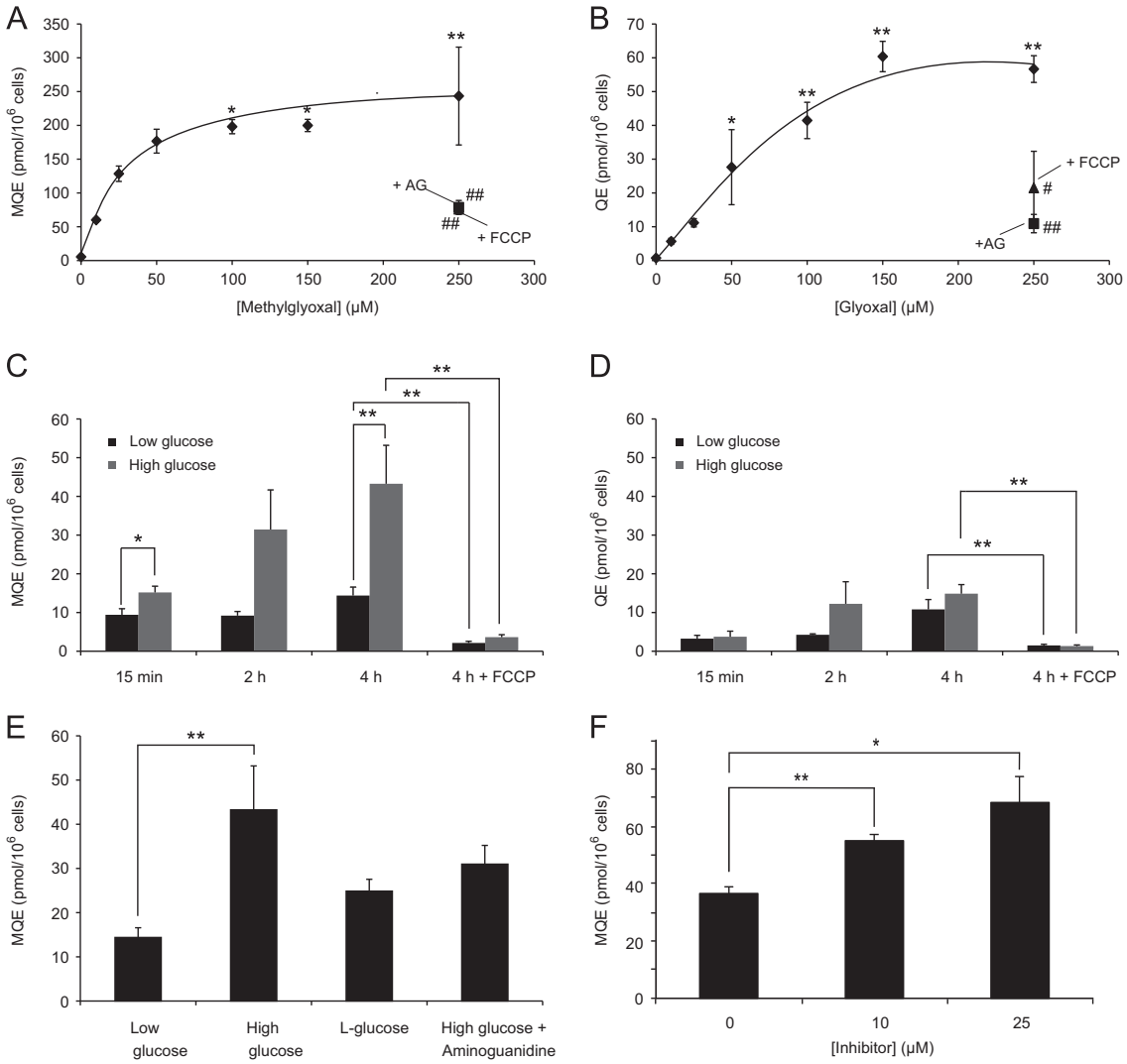

Fig. 9. Quantification of MQE and QE in cells. (A, B) BAECs were incubated with 2 μM MitoG for 1 h and sometimes supplemented with 10 mM AG or 2 μM FCCP. (A) Methylglyoxal or (B) glyoxal were then added, and after a further 3 h incubation, the levels of MQE and QE in the cell layers were determined by LC–MS/MS relative to deuterated ISs. (C, D) BAECs were incubated in media containing low (5 mM) or high (30 mM) D-glucose with 2 μM MitoG for the times indicated. Levels of (C) MQE and (D) QE in the cell layers were determined by LC–MS/MS relative to deuterated ISs. Results are means ± SE of four independent experiments. (E) BAECs were incubated for 4 h in the presence of 2 μM MitoG in media containing 5 mM D-glucose (low), 30 mM D-glucose (high), 5 mM D-glucose/25 mM L-glucose (L-glucose), or 30 mM D-glucose/10 mM aminoguanidinium. Levels of MQE in the cell layers were determined by LC–MS/MS relative to deuterated ISs. (F) BAECs were incubated in media containing high (30 mM) D-glucose with 2 μM MitoG for 4 h with the indicated concentrations of the glyoxalase I inhibitor bromobenzyl glutathione cyclopentyl diester. Levels of MQE in the cell layers were then determined by LC–MS/MS relative to deuterated ISs. Results are means ± SE of three (A, B) or four (C–E) independent experiments. $^{*}P < 0.05$ or $^{**}P < 0.01$, relative to untreated (A, B) or indicated (C–E) controls; $\#P < 0.05$ or $\#\#P < 0.01$ relative to cells treated with 250 μM 1,2-dicarbonyl.

Akita mice than in wild-type mice, and this increase in blood glucose correlated with a significant increase in both the MQE and the QE MitoG adducts, normalized to creatinine (Figs. 10A and B). These data suggest that MitoG can be used as a probe for the formation of methylglyoxal and glyoxal under conditions of pathologically relevant hyperglycemia in vivo.

Discussion

Disruption of mitochondrial function has been proposed to play a role in pathologies associated with hyperglycemia. One plausible pathway by which this may occur is through damaging glycation reactions to mitochondrial components by the reactive 1,2-dicarbonyls methylglyoxal and glyoxal. However, the importance of this pathway was difficult to assess in cells and in vivo because of the uncertainties about the levels of methylglyoxal and glyoxal that occur within mitochondria during hyperglycemia. Here we have developed a mass spectrometry approach to measure changes in the levels of these reactive 1,2-dicarbonyls within mitochondria in cells and in vivo.

We found that the combination of an *o*-phenylenediamine with a TPP moiety led to a molecule that accumulated within mitochondria, where it reacted with methylglyoxal and glyoxal to form stable products. These products could then be extracted from cells and biological fluids and analyzed by LC–MS/MS relative to stable isotope internal standards. The selectivity of this assessment for methylglyoxal and glyoxal was based on the identification of the products by tandem mass spectrometry, and this was further demonstrated by the changes in their levels on pharmacological inhibition of the glyoxalase system and by addition of the dicarbonyl trap aminoguanidine. The ability of the TPP moiety to locate compounds to mitochondria in cells and in vivo is well established, suggesting that the formation of MQE/QE occurs predominantly because of the reaction with methylglyoxal/glyoxal within the mitochondrial matrix. This is supported by the inhibition of the formation of MQE/QE by

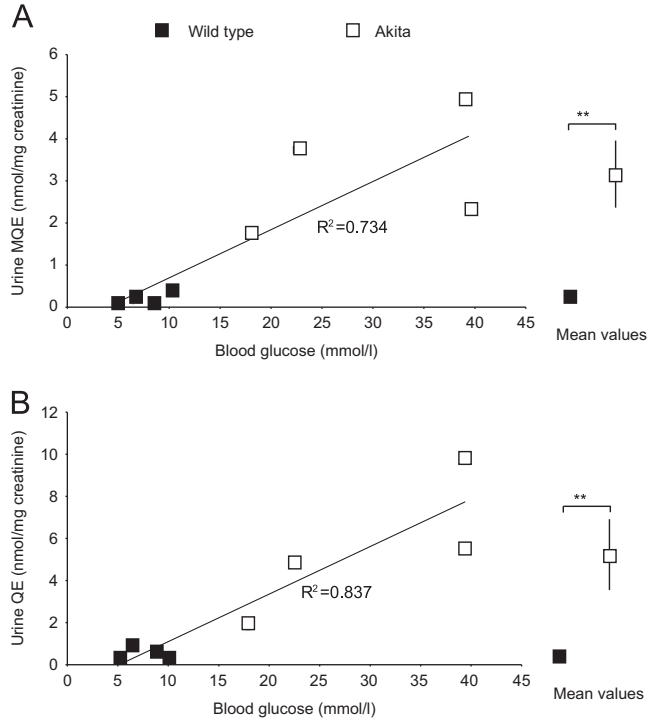

Fig. 10. Quantification of mitochondrial dicarbonyls in vivo. The levels of (A) MQE and (B) QE were quantified in urine of wild-type and Akita mice relative to creatinine and compared with blood glucose levels of these mice. MitoG (100 nmol) was administered by tail vein injection in both wild-type and Akita mice. After 4–6 h, blood glucose, urinary creatinine, and urinary MQE/QE levels were measured. The data to the right of the plots are the means ± SE of the two conditions. $^{**}P < 0.01$.

addition of the uncoupler FCCP, which decreases the uptake of MitoG into mitochondria. Furthermore, as the reaction between MitoG and methylgloxal/glyoxal is second order, the ~1000-fold concentration of MitoG within mitochondria will mean that the rate of formation of MQE/QE will be greater inside mitochondria by a similar factor. Thus formation of MQE/QE within a cell or tissue is largely due to changes in the amount of methylglyoxal/glyoxal within mitochondria. However, other reactive species within biological systems such as nitric oxide or reactive aldehydes such as 4-hydroxynonenal may also react with and deplete MitoG, although these reactions will not produce the diagnostic products formed from the reaction with glyoxal/methylglyoxal. Furthermore, although this approach will report on mitochondrial dicarbonyl exposure, it does not indicate the cellular source of the methylglyoxal/glyoxal, and they may be largely produced in the cytosol with subsequent diffusion into mitochondria.

The ability to use MitoG within living mice to generate MQE/QE as exomarkers to assess the changes in dicarbonyls that occurred within a model of type I diabetes was an important step. This suggests that this approach will be useful in assessing the role of reactive dicarbonyls in the mitochondrial damage associated with diabetes and in developing specific therapies. One limitation of MitoG is that it is not possible to normalize for tissue uptake because of the decomposition of MitoG over time in aerobic tissues. Thus changes in the uptake of MitoG into the tissue, for example by pathological alterations in mitochondrial membrane potential due to hyperglycemia, might lead to changes in the accumulation of the exomarker distinct from changes in organelle glyoxal concentration, and work is under way to circumvent this limitation.

The findings in Figs. 9 and 10 show that the formation of MQE and QE from MitoG increased dramatically under conditions of hyperglycemia both in cells and in vivo, indicating that there is a large increase in the amount of methylglyoxal/glyoxal in mitochondria under these conditions. This is consistent with mitochondrial glycation due to the accumulation of methylglyoxal/glyoxal in the matrix contributing to the mitochondrial disruption seen in hyperglycemia. To conclude, we have developed a new mitochondria-targeted mass spectrometric approach to assess levels of reactive dicarbonyls within mitochondria in cells and in vivo. This will be of use in assessing the contribution of these damaging species to mitochondrial dysfunction in diabetes and aging.

Acknowledgments

This work was supported by the Medical Research Council (UK), by the Foundation for Research, Science and Technology (NZ), by Grant BB/I012826/1 from the BBSRC (to R.C.H. and M.P.M.), and by the NIH (Grant DK075865 to V.D.U.). We thank Dr. Helena Cochemé for assistance with the figures.

Appendix A. Supplementary material

Supplementary data associated with this article can be found in the online version at http://dx.doi.org/10.1016/j.freeradbiomed.2013.11.025.

References

[1] Brownlee, M. Negative consequences of glycation. *Metab. Clin. Exp* **49:**9–13; 2000.
[2] Thornalley, P. J. Protein and nucleotide damage by glyoxal and methylglyoxal in physiological systems—role in ageing and disease. *Drug Metab. Drug Interact* **23:**125–150; 2008.
[3] Pun, P. B.; Murphy, M. P. Pathological significance of mitochondrial glycation. *Int. J. Cell Biol.* **2012:**843505; 2012.
[4] Brownlee, M. Biochemistry and molecular cell biology of diabetic complications. *Nature* **414:**813–820; 2001.
[5] Rabbani, N.; Thornalley, P. J. Glyoxalase in diabetes, obesity and related disorders. *Semin. Cell Dev. Biol.* **22:**309–317; 2011.
[6] Phillips, S. A.; Thornalley, P. J. The formation of methylglyoxal from triose phosphates—investigation using a specific assay for methylglyoxal. *Eur. J. Biochem.* **212:**101–105; 1993.
[7] Casazza, J. P.; Felver, M. E.; Veech, R. L. The metabolism of acetone in rat. *J. Biol. Chem.* **259:**231–236; 1984.
[8] Lo, T. W. C.; Westwood, M. E.; Mclellan, A. C.; Selwood, T.; Thornalley, P. J. Binding and modification of proteins by methylglyoxal under physiological conditions—a kinetic and mechanistic study with N-alpha-acetylarginine, N-alpha-acetylcysteine, and N-alpha-acetyllysine, and bovine serum-albumin. *J. Biol. Chem.* **269:**32299–32305; 1994.
[9] Chaplen, F. W.; Fahl, W. E.; Cameron, D. C. Evidence of high levels of methylglyoxal in cultured Chinese hamster ovary cells. *Proc. Natl. Acad. Sci. USA* **95:**5533–5538; 1998.
[10] Thornalley, P. J.; Battah, S.; Ahmed, N.; Karachalias, N.; Agalou, S.; Babaei-Jadidi, R.; Dawnay, A. Quantitative screening of advanced glycation endproducts in cellular and extracellular proteins by tandem mass spectrometry. *Biochem. J.* **375:**581–592; 2003.
[11] Thornalley, P. J.; Waris, S.; Fleming, T.; Santarius, T.; Larkin, S. J.; Winklhofer-Roob, B. M.; Stratton, M. R.; Rabbani, N. Imidazopurinones are markers of physiological genomic damage linked to DNA instability and glyoxalase 1-associated tumour multidrug resistance. *Nucleic Acids Res.* **38:**5432–5442; 2010.
[12] Kingkeohoi, S.; Chaplen, F. W. R. Analysis of methylglyoxal metabolism in CHO cells grown in culture. *Cytotechnology* **48:**1–13; 2005.
[13] Dhar, A.; Desai, K.; Liu, J. H.; Wu, L. Y. Methylglyoxal, protein binding and biological samples: are we getting the true measure? *J. Chromatogr. B* **877:**1093–1100; 2009.
[14] Thornalley, P. J. The glyoxalase system: new developments towards functional characterization of a metabolic pathway fundamental to biological life. *Biochem. J* **269:**1–11; 1990.
[15] Morcos, M.; Du, X.; Pfisterer, F.; Hutter, H.; Sayed, A. A.; Thornalley, P.; Ahmed, N.; Baynes, J.; Thorpe, S.; Kukudov, G.; Schlotterer, A.; Bozorgmehr, F.; El Baki, R. A.; Stern, D.; Moehrlen, F.; Ibrahim, Y.; Oikonomou, D.; Hamann, A.; Becker, C.; Zeier, M.; Schwenger, V.; Miftari, N.; Humpert, P.; Hammes, H. P.; Buechler, M.; Bierhaus, A.; Brownlee, M.; Nawroth, P. P. Glyoxalase-1 prevents mitochondrial protein modification and enhances lifespan in Caenorhabditis elegans. *Aging Cell* **7:**260–269; 2008.

[16] Green, K.; Brand, M. D.; Murphy, M. P. Prevention of mitochondrial oxidative damage as a therapeutic strategy in diabetes. *Diabetes* **53(Suppl. 1):**S110–118; 2004.
[17] Yoon, Y.; Galloway, C. A.; Jhun, B. S.; Yu, T. Mitochondrial dynamics in diabetes. *Antioxid. Redox Signaling* **14:**439–457; 2011.
[18] Newsholme, P.; Gaudel, C.; Krause, M. Mitochondria and diabetes: an intriguing pathogenetic role. *Adv. Exp. Med. Biol.* **942:**235–247; 2012.
[19] Baynes, J. W.; Thorpe, S. R. Role of oxidative stress in diabetic complications—a new perspective on an old paradigm. *Diabetes* **48:**1–9; 1999.
[20] Rosca, M. G.; Mustata, T. G.; Kinter, M. T.; Ozdemir, A. M.; Kern, T. S.; Szweda, L. I.; Brownlee, M.; Monnier, V. M.; Weiss, M. F. Glycation of mitochondrial proteins from diabetic rat kidney is associated with excess superoxide formation. *Am. J. Physiol.* **289:**F420–F430; 2005.
[21] Ceriello, A.; Ihnat, M. A.; Thorpe, J. E. The "metabolic memory": is more than just tight glucose control necessary to prevent diabetic complications? *J. Clin. Endocrinol. Metab.* **94:**410–415; 2009.
[22] Ray, S.; Dutta, S.; Halder, J.; Ray, M. Inhibition of electron flow-through complex I of the mitochondrial respiratory-chain of Ehrlich ascites-carcinoma cells by methylglyoxal. *Biochem. J* **303:**69–72; 1994.
[23] Biswas, S.; Ray, M.; Misra, S.; Dutta, D. P.; Ray, S. Selective inhibition of mitochondrial respiration and glycolysis in human leukaemic leucocytes by methylglyoxal. *Biochem. J.* **323(Pt 2):**343–348; 1997.
[24] Rosca, M. G.; Monnier, V. M.; Szweda, L. I.; Weiss, M. F. Alterations in renal mitochondrial respiration in response to the reactive oxoaldehyde methylglyoxal. *Am. J. Physiol.* **283:**F52–59; 2002.
[25] Murphy, M. P. Development of lipophilic cations as therapies for disorders due to mitochondrial dysfunction. *Expert Opin. Biol. Ther* **1:**753–764; 2001.
[26] Smith, R. A. J.; Hartley, R. C.; Cocheme, H. M.; Murphy, M. P. Mitochondrial pharmacology. *Trends Pharmacol. Sci.* **33:**341–352; 2012.
[27] Smith, R. A. J.; Porteous, C. M.; Gane, A. M.; Murphy, M. P. Delivery of bioactive molecules to mitochondria in vivo. *Proc. Natl. Acad. Sci. USA* **100:**5407–5412; 2003.
[28] Chaplen, F. W.; Fahl, W. E.; Cameron, D. C. Method for determination of free intracellular and extracellular methylglyoxal in animal cells grown in culture. *Anal. Biochem.* **238:**171–178; 1996.
[29] Yamaguchi, M.; Hara, S.; Nakamura, M. Determination of methylglyoxal in mouse blood by liquid chromatography with fluorescence detection. *Anal. Chim. Acta* **221:**163–166; 1989.
[30] Cochemé, H. M.; Logan, A.; Prime, T. A.; Abakumova, I.; Quin, C.; McQuaker, S. J.; Patel, J. V.; Fearnley, I. M.; James, A. M.; Porteous, C. M.; Smith, R. A. J.; Hartley, R. C.; Partridge, L.; Murphy, M. P. Using the mitochondria-targeted ratiometric mass spectrometry probe MitoB to measure H_2O_2 in living *Drosophila*. *Nat. Protoc.* **7:**946–958; 2012.
[31] Cochemé, H. M.; Quin, C.; McQuaker, S. J.; Cabreiro, F.; Logan, A.; Prime, T. A.; Abakumova, I.; Patel, J. V.; Fearnley, I. M.; James, A. M.; Porteous, C. M.; Smith, R. A. J.; Saeed, S.; Carre, J. E.; Singer, M.; Gems, D.; Hartley, R. C.; Partridge, L.; Murphy, M. P. Measurement of H_2O_2 within living *Drosophila* during aging using a ratiometric mass spectrometry probe targeted to the mitochondrial matrix. *Cell Metab.* **13:**340–350; 2011.
[32] Carrigan, C. N.; Bartlett, R. D.; Esslinger, C. S.; Cybulski, K. A.; Tongcharoensirikul, P.; Bridges, R. J.; Thompson, C. M. Synthesis and in vitro pharmacology of substituted quinoline-2,4-dicarboxylic acids as inhibitors of vesicular glutamate transport. *J. Med. Chem.* **45:**2260–2276; 2002.
[33] Fanta, P. E.; Tarbell, D. S. 2-Nitro-4-methoxyaniline. *Org. Synth.* **25:**78–80; 1945.
[34] Barton, J. K.; Shao, F.; Elias, B.; Lu, W. Synthesis and characterization of iridium (III) cyclometalated complexes with oligonucleotides: insights into redox reactions with DNA. *Inorg. Chem.* **46:**10187–10199; 2007.
[35] Thornalley, P. J.; Edwards, L. G.; Kang, Y.; Wyatt, C.; Davies, N.; Ladan, M. J.; Double, J. Antitumour activity of *S*-*p*-bromobenzylglutathione cyclopentyl diester in vitro and in vivo: inhibition of glyoxalase I and induction of apoptosis. *Biochem. Pharmacol.* **51:**1365–1372; 1996.
[36] Twibanire, J. D.; Grindley, T. B. Efficient and controllably selective preparation of esters using uronium-based coupling agents. *Org. Lett.* **13:**2988–2991; 2011.
[37] Kelso, G. F.; Porteous, C. M.; Coulter, C. V.; Hughes, G.; Porteous, W. K.; Ledgerwood, E. C.; Smith, R. A. J.; Murphy, M. P. Selective targeting of a redox-active ubiquinone to mitochondria within cells—antioxidant and antiapoptotic properties. *J. Biol. Chem.* **276:**4588–4596; 2001.
[38] Asin-Cayuela, J.; Manas, A. R.; James, A. M.; Smith, R. A. J.; Murphy, M. P. Fine-tuning the hydrophobicity of a mitochondria-targeted antioxidant. *FEBS Lett.* **571:**9–16; 2004.
[39] Choi, S. W.; Gerencser, A. A.; Nicholls, D. G. Bioenergetic analysis of isolated cerebrocortical nerve terminals on a microgram scale: spare respiratory capacity and stochastic mitochondrial failure. *J. Neurochem.* **109:**1179–1191; 2009.
[40] Dranka, B. P.; Benavides, G. A.; Diers, A. R.; Giordano, S.; Zelickson, B. R.; Reily, C.; Zou, L.; Chatham, J. C.; Hill, B. G.; Zhang, J.; Landar, A.; Darley-Usmar, V. M. Assessing bioenergetic function in response to oxidative stress by metabolic profiling. *Free Radic. Biol. Med.* **51:**1621–1635; 2011.
[41] Hill, B. G.; Benavides, G. A.; Lancaster Jr J. R.; Ballinger, S.; Dell'Italia, L.; Jianhua, Z.; Darley-Usmar, V. M. Integration of cellular bioenergetics with mitochondrial quality control and autophagy. *Biol. Chem.* **393:**1485–1512; 2012.
[42] Brand, M. D.; Nicholls, D. G. Assessing mitochondrial dysfunction in cells. *Biochem. J.* **435:**297–312; 2011.
[43] Yoshioka, M.; Kayo, T.; Ikeda, T.; Koizumi, A. A novel locus, Mody4, distal to D7Mit189 on chromosome 7 determines early-onset NIDDM in nonobese C57BL/6 (Akita) mutant mice. *Diabetes* **46:**887–894; 1997.
[44] Izumi, T.; Yokota-Hashimoto, H.; Zhao, S.; Wang, J.; Halban, P. A.; Takeuchi, T. Dominant negative pathogenesis by mutant proinsulin in the Akita diabetic mouse. *Diabetes* **52:**409–416; 2003.
[45] Chacko, B. K.; Reily, C.; Srivastava, A.; Johnson, M. S.; Ye, Y.; Ulasova, E.; Agarwal, A.; Zinn, K. R.; Murphy, M. P.; Kalyanaraman, B.; Darley-Usmar, V. Prevention of diabetic nephropathy in $Ins^{2(+/)(AkitaJ)}$ mice by the mitochondria-targeted therapy MitoQ. *Biochem. J.* **432:**9–19; 2010.
[46] Murata-Kamiya, N.; Kamiya, H. Methylglyoxal, an endogenous aldehyde, crosslinks DNA polymerase and the substrate DNA. *Nucleic Acids Res.* **29:**3433–3438; 2001.
[47] Murata-Kamiya, N.; Kamiya, H.; Kaji, H.; Kasai, H. Mutations induced by glyoxal and methylglyoxal in mammalian cells. *Nucleic Acids Symp. Ser.* **44:**3–4; 2000.
[48] Pampati, P. K.; Suravajjala, S.; Dain, J. A. Monitoring nonenzymatic glycation of human immunoglobulin G by methylglyoxal and glyoxal: a spectroscopic study. *Anal. Biochem.* **408:**59–63; 2011.
[49] Fedoronko, M.; Konigstein, J.; Linek, K. Determination of dl-glyceraldehyde, dihydroxyacetone and methylglyoxal in a mixture. *J. Electroanal. Chem. Interfacial Electrochem.* **14:**357–367; 1967.
[50] Chouchani, E. T.; Methner, C.; Nadtochiy, S. M.; Logan, A.; Pell, V. R.; Ding, S.; James, A. M.; Cochemé, H. M.; Reinhold, J.; Lilley, K. S.; Partridge, L.; Fearnley, I. M.; Robinson, A. J.; Hartley, R. C.; Smith, R. A. J.; Krieg, T.; Brookes, P. S.; Murphy, M. P. Cardioprotection by S-nitrosation of a cysteine switch on mitochondrial complex I. *Nat. Med.* **19:**753–759; 2013.
[51] Logan, A.; Cochemé, H. M.; Boon Li Pun, P.; Apostolova, N.; Smith, R. A. J.; Larsen, L.; Larsen, D. S.; James, A. M.; Fearnley, I. M.; Rogatti, S.; Prime, T. A.; Finichiu, P.; Dare, A.; Chouchani, E. T.; Pell, V. R.; Methner, C.; Quin, C.; McQuaker, S. J.; Krieg, T.; Hartley, R. C.; Murphy, M. P. *Biochim. Biophys. Acta* **1840:**923–930; 2014.
[52] Porteous, C. M.; Logan, A.; Evans, C.; Ledgerwood, E. C.; Menon, D. K.; Aigbirhio, F.; Smith, R. A.; Murphy, M. P. Rapid uptake of lipophilic triphenylphosphonium cations by mitochondria in vivo following intravenous injection: implications for mitochondria-specific therapies and probes. *Biochim. Biophys. Acta* **1800:**1009–1017; 2010.
[53] Li, Y.; Zhang, H.; Fawcett, J. P.; Tucker, I. G. Effect of cyclosporin A on the pharmacokinetics of mitoquinone (MitoQ10), a mitochondria-targeted antioxidant, in rat. *Asian J. Pharm. Sci.* **5:**106–113; 2010.